Short communication

Hexagonal Mo/V/W mixed oxide as a catalyst for the partial oxidation of methacrolein to methacrylic acid

Maximilian Sennerich[a], Peter Weidler[b], Bettina Kraushaar-Czarnetzki[a],[*]

[a] *Institute of Chemical Process Engineering CVT, Karlsruhe Institute of Technology, Campus South, 76131 Karlsruhe, Germany*
[b] *Institute of Functional Interfaces IFG, Karlsruhe Institute of Technology, Campus North, 76344 Eggenstein-Leopoldshafen, Germany*

ARTICLE INFO

ABSTRACT

This work evaluates for the first time the catalytic performance of a hexagonal Mo/V/W mixed oxide, the so-called h-phase, in the partial oxidation of methacrolein to methacrylic acid. Three catalysts with different phase compositions were compared. One catalyst predominantly contained h-phase, a further consisted of the well-known M1 phase, and a third catalyst was composed of both, h-phase and M1, in similar amounts. The selectivity of the h-phase catalyst is comparable to that of M1.

1. Introduction

Methacrylic acid (MAA) and several of its esters are important intermediates for acrylic polymers which are used in the manufacturing of transparent plastics, glues, thickeners and lacquers [1]. MAA is synthesized by selective oxidation of methacrolein (MAC) usually carried out over heteropoly acid (HPA) catalysts, which combine high activity and selectivity towards MAA [2]. However, the HPA lifetime under typical reaction conditions with less than one year is unsatisfactory. The low stability of HPA has triggered the search for alternative catalysts that combine high selectivity to MAA with improved long-term stability.

In the partial oxidation of acrolein (ACR) to acrylic acid (AA), Mo/V/W mixed oxide (MO) catalysts are used with great success; in the corresponding processes, runtimes of more than three years are typical [2]. Since acrolein and methacrolein are homologue α,β-unsaturated carbonyl compounds, it is an obvious thought to explore MO-type catalysts also in the MAC oxidation. So far, there are only a few studies involving mixed oxide catalyst in the partial oxidation of MAC to MAA [2–4]. The materials under investigation were nanocrystalline/amorphous $(Mo,V,W)_5O_{14}$ and the so-called M1 phase, both being considered as active phases in the ACR oxidation catalysis [2,3,5–10]. In the oxidation of MAC to MAA, however, these MO-type catalysts exhibited poor selectivities ($S_{MAA,MAC} \approx 35\%$ at $X_{MAC} \approx 40\%$) [2–4]. A hexagonal Mo/V/W mixed oxide denoted as h-phase is also known as a highly active ACR oxidation catalyst [11,12] but has not yet been evaluated in the MAC oxidation.

2. Experimental

2.1. Catalyst preparation

2.1.1. Catalyst A

The hexagonal $(Mo,V,W)O_3$ catalyst was prepared by evaporation crystallization from an aqueous precursor solution. 29.76 g ammonium heptamolybdate (Alfa Aesar, 99%), 4.93 g ammonium metavanadate (Merck, 99%) and 5.32 g ammonium metatungstate (Honeywell, 99%) were dissolved in 1000 mL demineralized water in order to obtain $Mo_8V_2W_1O_x$. Nitric acid was added to adjust the pH value to 5. The solution was stirred at 85 °C for 90 min under reflux. After that, the water was completely evaporated at 60 °C under atmospheric pressure. Consequently, the yellow colored solid precursor crystallized. The precursor was crushed into powder form and calcinated under nitrogen atmosphere in a calcination oven (Carbolite© HTR 11/150). The powder was heated to 325 °C with a heating rate of 2 K/min, held for 240 min, heated further to 400 °C with 2 K/min and held for another 10 min until it was rapidly cooled down by shutting off the heater. During the calcination process, the powder turned black. To increase the catalyst surface area and the catalytic performance, the catalyst was brought into suspension with demineralized water with a ratio of 10 g catalyst per 100 mL of water. The suspension was evaporated under stirring at a temperature of 60 °C. Afterwards the catalyst was crushed into powder and calcinated again as previously described.

2.1.2. Catalyst B

The catalyst containing M1 phase and hexagonal phase was

Notation

Abbreviations

FID	flame ionization detector
HAc	acetic acid
HPA	heteropoly acid
MAA	methacrylic acid
MAC	methacrolein
MO	mixed oxide
TCD	thermal conductivity detector

Symbols

A_{BET}	specific surface area ($m^2 \cdot g^{-1}$)

$C_{MAC,s}$	MAC concentration on the catalyst surface ($mol \cdot m^{-3}$)
$C_{MAC,g}$	MAC concentration in the gas phase ($mol \cdot m^{-3}$)
F_i	integrated area in XRD diffractogram ($-$)
$k_{F,i}$	surface specific reaction rate coefficient ($m \cdot s^{-1}$)
$k_{m,I}$	mass specific reaction rate coefficient ($m^3 \cdot kg^{-1} \cdot s^{-1}$)
$\dot{n}_i$	molar flow of component i ($mol \cdot s^{-1}$)
$\dot{n}_{i,0}$	molar flow of component i at the inlet ($mol \cdot s^{-1}$)
$^R S_i$	carbon-based reactor selectivity to component i ($-$)
TOS	time on stream (h)
$\dot{V}$	total volumetric inlet flow ($m^3 \cdot s^{-1}$)
Wz	Weisz number for inner mass transfer limitation ($-$)
X_i	conversion of component i ($-$)
z_i	carbon number of component i ($-$)
τ_{mod}	modified residence time at standard conditions ($kg \cdot s \cdot m^{-3}$)

obtained by means of spray drying according to example 1) in [13]. An aqueous precursor containing 29.76 g ammonium heptamolybdate (Alfa Aesar, 99%), 4.93 g ammonium metavanadate (Merck, 99%) and 2.66 g ammonium metatungstate (Honeywell, 99%) per 1000 mL of demineralized water was spray dried. The sprayed precursor powder was then kneaded with added water and calcined similar to catalyst A.

2.1.3. Catalyst C

The M1 phase was acquired through hydrothermal synthesis in an autoclave following the procedure of example 2) in [14]. 11.61 g ammonium heptamolybdate (Alfa Aesar, 99%) and 1.01 g ammonium metatungstate (Honeywell, 99%) were dissolved in 120 mL of demineralized water (solution A). Another solution containing 3.97 g vanadium sulfate oxide hydrate (Alfa Aesar, 99.9%) in 120 mL

demineralized water was prepared (solution B). Solution A was slowly added to solution B. The pH of solution AB was adjusted to 2.2 with sulfuric acid before it was thermally treated in an autoclave at 175 °C for 24 h. The calcination was also conducted under nitrogen atmosphere. The catalyst was heated to 500 °C with a heating rate of 2 K/min and held for 120 min until it was cooled down by shutting off the heaters.

All catalysts were shaped in the same way. They were grinded into a fine powder before they were pressed into cylindrical pellets (length 15 mm, diameter 11 mm), crushed and sieved. Catalytic tests were performed with a particle fraction of 0.71 mm to 1.25 mm diameter. To check on external mass transfer limitation effects, the concentration gradient of MAC between gas phase and catalyst surface was calculated (Supplementary Material A.1). Possible mass transfer limitations in the
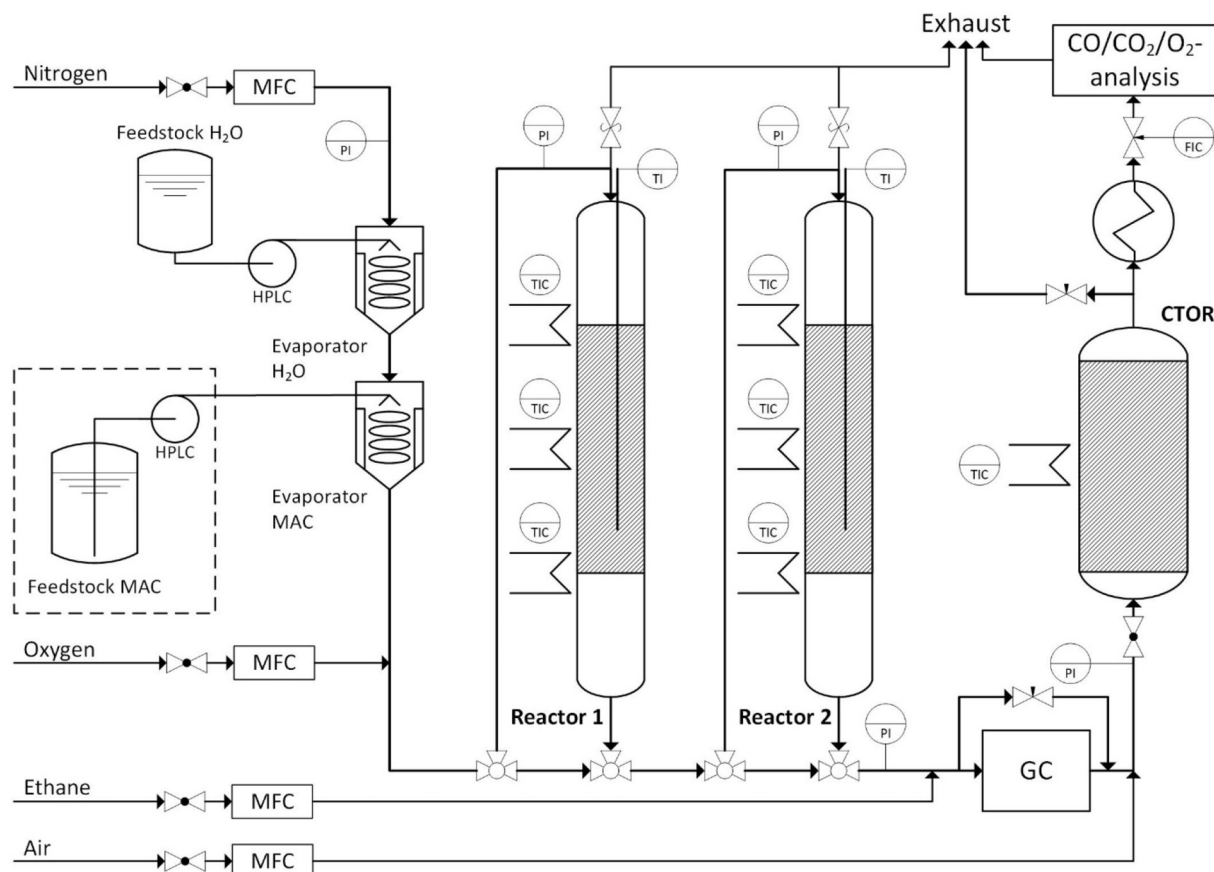
Fig. 1. Simplified flow scheme of the lab scale plant.

inter-crystalline voids (mesopores) were inspected by calculating the Weisz number Wz (Supplementary Material A.2). Both, internal and external mass transfer limitations could be ruled out.

2.2. Reaction unit

Catalytic experiments were carried out in a lab scale plant with two tubular fixed-bed reactors in series (Fig. 1). All gases were dosed with thermal mass flow controllers (Brooks GF40, Brooks SLA5850). Pre-heated nitrogen (Air Liquide, 99.999%) entered the water evaporator. Water was fed by a HPLC pump (Bischoff 3350) through a capillary for additional back-pressure and entered the water evaporator at 80 °C. Downstream the MAC evaporation was accomplished with an identical evaporator, which was fed by another HPLC pump (Bischoff 3350) at a temperature of 125 °C. In contrast to the water evaporation, the back-pressure generation was achieved with a HPLC back pressure regulator (Vici JR-BPR2) at pressures > 30 bar(a). Oxygen (Air Liquide, 99.95%) was added after the MAC evaporator to prevent the occurrence of an explosive atmosphere during undesired evaporation instabilities. Subsequently the gas mix entered the PFR reactors, which could be individually bypassed. The feed stream was measured with both reactors in bypassed position. The two reactors in this setup allowed measuring two modified residence times (eq. 1) with the same feed stream. Each reactor was equipped with a blow off valve in case the pressure exceeded 4 bar(a). After the reactors, the gas stream was mixed with ethane (Air Liquide, 99.95%) as an internal standard for the online gas chromatograph (GC, Agilent 6890 N) equipped with a FID – and TCD detector. A needle valve in the main exhaust pipe allowed for pressure control and ensured a constant flow rate through the GC sampling loop, which was connected to the process with a 1/16″ bypass tube. After the GC all organic components were completely oxidized in a catalytic total oxidation reactor (CTOR, 0.25% m/m Pd on γ-Al$_2$O$_3$) followed by on-line IR and paramagnetic detectors for carbon oxides and oxygen (ABB, AO2020, Uras 26, Magnos 206) in the exhaust gases. An upstream cooling trap removed water from the gas stream, which could damage the IR detector. This setup ensured a toxic free gas release into the environment and a constant monitoring of the plant carbon balance.

Both reactors (stainless steel, length 350 mm, and inner diameter 16 mm) were heated with three heating zones. To ensure ideal plug-flow and an evenly distributed temperature profile, coarse silicon carbide particles of 1 mm were placed above and below the catalyst bed. The catalyst was embedded in fine silicon carbide particles with 0.2 mm diameter. Isothermal conditions (ΔT_{max} = 2 K) were ensured in each experiment by a coaxially displaceable thermocouple (Ni/Cr–Ni).

Catalytic performance tests were conducted at a temperature of 300 °C and a pressure of 1.5 bar(a) with a total volumetric inlet flow between 300 and 1200 mL$_N$/min and a modified residence time between 500 and 4000 kg·s/m^3. The inlet stream composition was 3.4% v/v MAC, 6.8% v/v O$_2$, 21% v/v H$_2$O and 68.8% v/v N$_2$. The modified residence time is defined as the quotient of the total mass of active component and the volumetric inlet flow (Eq. 1) at standard conditions; values were varied such that a conversion range of from 30% to 80% was covered.

$$\tau_{mod} = \frac{m_{Kat}}{\dot{V}(p_N, T_N)} \quad (1)$$

Before taking steady-state measurements, each catalyst was held for 72 h TOS under reaction conditions. All experiments were conducted for at least 2 h to have a sufficiently large number of GC measurements. For the evaluation of the measurements, the MAC conversion and the carbon balanced reactor selectivity of the products were calculated. The conversion is defined in Eq. 2 as:

$$X_{MAC} = \frac{\dot{n}_{MAC,0} - \dot{n}_{MAC}}{\dot{n}_{MAC,0}} \quad (2)$$

where $\dot{n}_i$ is the molar flow and z_i the number of carbon atoms of component i. The reactor selectivity to the product i (Eq. 3) was calculated as:

$$^R S_i = \frac{(\dot{n}_i - \dot{n}_{i,0}) \cdot z_i}{(\dot{n}_{MAC,0} - \dot{n}_{MAC}) \cdot z_{MAC}} \quad (3)$$

The surface specific rate coefficient of the catalysts was estimated by assuming a first order reaction of methacrolein. Integration and transformation of the PFR balance leads to the mass specific reaction rate coefficient k$_m$ (Eq. 4):

$$-\ln(1 - X_{MAC}) = k_m \cdot \tau_{mod} \quad (4)$$

The surface specific rate coefficient k$_F$ (Eq. 5) is obtained as follows:

$$k_F = \frac{k_m}{A_{BET}} \quad (5)$$

In addition to the surface specific rate coefficient, the crystallinity corrected mass specific rate coefficient k$_C$ can be calculated according to Eq.6:

$$k_C = \frac{k_m}{crystallinity} \quad (6)$$
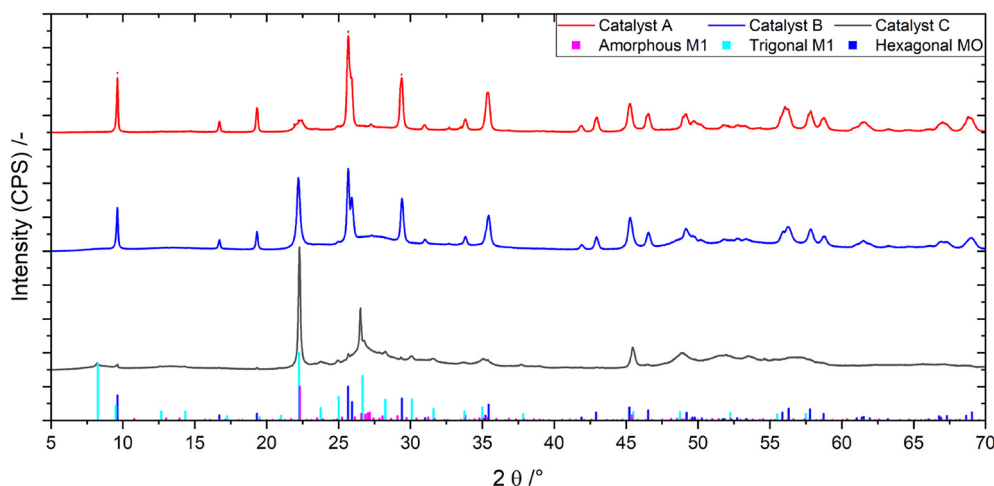
Fig. 2. XRD patterns of catalysts A (red), B (blue) and C (black) together with the characteristic XRD reflections of "amorphous" M1, trigonal M1 and h-phase (bottom). (For interpretation of the references to colour in this figure legend, the reader is referred to the web version of this article.)

2.3. Catalyst characterization

The elemental analysis was accomplished by means of wavelength dispersive X-ray Fluorescence (WDXRF) spectroscopy (Pioneer S4, Bruker AXS).

X-ray diffraction (XRD) measurements were conducted with a Bruker D8 Advance diffractometer equipped with a LynxEye XD detector. Cu kα radiation with a step with of 0.015° in a range from 5 to 95° was used. XRD data evaluation was performed with the software DIFFRAC.SUITE EVA from Bruker. Catalyst crystallinity was estimated using Eq. (7), where F represents the respective integrated XRD peak area.

$$crystallinity = \frac{F_{total} - F_{amorphous}}{F_{total}} \tag{7}$$

The catalysts' specific surface areas (A_{BET}) were determined by means of nitrogen physisorption according to the BET method using a Micromeritics PhysiSporption ASAP 2020. Scanning electron micrographs (SEM) were taken on a LEO1530. All samples were coated with a thin carbon film (5 nm) to prevent static charging.

3. Results and discussion

3.1. Catalyst characterization

XRD patterns of the three catalysts are shown in Fig. 2. The phase composition of the probes estimated by integration of the diffractograms is displayed in Table 1. The phase compositions reported in Table 1 refer only to the crystalline portions of the catalysts. Catalyst A is mostly composed of the hexagonal $(Mo,V,W)O_3$ (h-phase) and matches XRD patterns as reported by Kunert et al. [12,15]. The catalyst also contains a minor amount of a so-called amorphous M1 phase, to which the widened peak at 2θ ≈ 22.2° can be assigned. This amorphous M1 phase is reportedly not truly XRD amorphous, but rather lacks far-order in the a-b planes of the unit cell [5]. Furthermore, catalyst A contains a minor amount of orthorhombic MoO_3 (< 2% m/m). Catalyst B contains significant amounts of M1 besides h-phase. Catalyst C consists of amorphous and trigonal M1 phases. The trigonal M1 phase – in contrast to the amorphous M1 phase – features a far order in a-, b- and c-plane and exhibits a higher catalytic activity in the partial oxidation of acrolein with similar selectivity towards acrylic acid [5,9,10]. Impurities in catalyst C are minor amounts of hexagonal $(Mo,V,W)O_3$ (< 2% m/m) and of a $(Mo,V,W)_5O_{14}$ phase (< 3% m/m). The comparison of XRD patterns taken before and after catalytic testing for runtimes of at least 120 h indicated no phase changes.

H-phase and M1 phase share hexagonal channels as a morphologic similarity, and M1 exhibits additional heptagonal channels (Fig. 3). However, these narrow micropores are not accessible to feed molecules. BET surface areas (Table 1) and the isotherms of nitrogen ad- and desorption (Supplement Material) clearly show that these micropores are too narrow for nitrogen adsorption. Hence, the catalytic MAC conversion must take place on the external crystal surfaces. It is not exactly known so far how the metal ions are distributed over the lattice sites. This lack of knowledge is also reflected in Fig. 3 where all metal ions (Mo, V and W) are represented by blue balls.

Scanning electron micrographs of the catalysts have been enclosed in the Supplement. While catalyst C crystals exhibit a rod/needle like structure, which is characteristic for M1 phases [8,18], catalyst A shows an irregular surface with no visible rod crystallites. Catalyst B, containing both h- and M1-phase, combines the two morphologies.

3.2. Catalytic performance

Conversion and selectivity plots of the three catalysts are shown in Fig. 4. The main products of the partial oxidation of MAC are MAA, CO, CO_2 and acetic acid (HAc). Since the production ratio of CO and CO_2 was similar for all measurements, the carbon oxides were lumped together as CO_x. The CO_x and HAc selectivities can be found in the Supplement. Other mentionable byproducts are acetone and acrylic acid, which are not shown since their combined selectivity is below 5%. Both the h-phase catalyst A and the M1 phase catalyst C exceed catalyst B with a higher selectivity towards MAA, while catalyst B features the highest selectivity towards CO_x. All catalysts show roughly the same selectivity to acetic acid (supplementary Material A.6).

Remarkably, h-phase (catalyst A) and M1 (catalyst C) exhibit similar selectivity patterns. This is interesting since selective sites for the partial oxidation of unsaturated aldehydes have been ascribed to nanocrystalline/amorphous M1 and Mo_5O_{14}-phases so far [2,9,19]. The amorphous M1 phase seems to be less selective for MAA, since catalyst B, containing h-phase and amorphous M1 phase, performs worse than the h-phase catalyst A. Because of the lack of knowledge about the coordination of the metal ions and their precise location in both, M1 and h-phase, we refrain from speculations about possible structural similarities between M1 and h-phase as a cause for the similar catalytic performance. Also, the existence of micropores in both mixed oxides does not provide a straightforward explanation as these micropores are far too narrow to participate in diffusional mass transfer.

All catalysts showed a run-in behavior accompanied by a minor decrease in surface area and a slight drop in conversion within the first 72 h on stream. After the run-in period, the catalysts' activity and selectivity remained unchanged throughout the experiments. Catalyst activities after completion of the run-in period, i.e. in the steady state, are reported in Table 2 in terms of first order rated coefficients, which have been related either to the catalyst mass, to the specific surface area or to the mass and corrected for the crystallinity. While the mass specific catalyst activity coefficient increases from catalyst A to C, the surface specific activity k_F of catalyst A lies between catalyst B and C, with catalyst C also featuring the highest k_F value. When relating the catalyst activity to the crystallinity of the probes, catalyst A shows the lowest catalytic activity coefficient. Since it is unclear, how the amorphous and crystalline catalyst share contribute to the total specific surface area, the crystallinity and specific surface area cannot be used for a combined specific rate coefficient.

In this regard, the catalyst activity is not simply a function of specific surface area. As for the selectivity, the higher activity of the M1 phase catalyst C could be related to the trigonal M1 phase, which catalyst B does not contain.

4. Conclusions

The present work compared a hexagonal Mo/V/W phase with the well-known M1 phase in the selective oxidation of methacrolein to methacrylic acid. Three catalysts containing different amounts of hexagonal phase and M1 phase were synthesized. So far, the hexagonal

Table 1
Phase compositions, specific surface areas and elemental compositions of catalysts A, B, and C.*) figures refer to the crystalline portion of the catalyst.

Catalyst	Crystallinity (% m/m)	h-phase (% m/m)*	M1 phase (% m/m)*	A_{BET} (m^2/g)	Composition
A	≈ 79	> 95	< 5	13.9	$Mo_{8.00}V_{2.02}W_{1.02}$
B	≈ 68	≈ 55	≈ 45	20.6	$Mo_{8.00}V_{2.01}W_{0.48}$
C	≈ 58	< 5	> 95	25.8	$Mo_{8.00}V_{2.34}W_{0.77}$
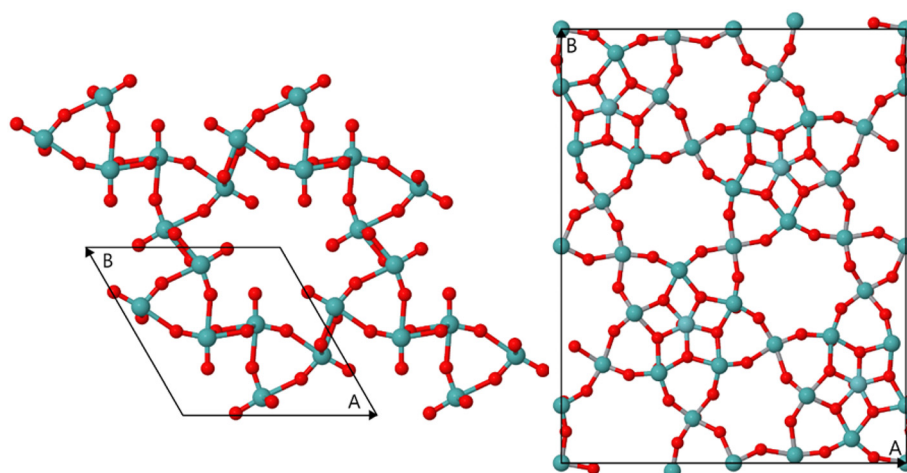
Fig. 3. Crystal structure of h-Phase [16] (left) and M1 phase [8] (right) from ICSD Database [17]. Blue: Mo,V,W; red: O. (For interpretation of the references to colour in this figure legend, the reader is referred to the web version of this article.)
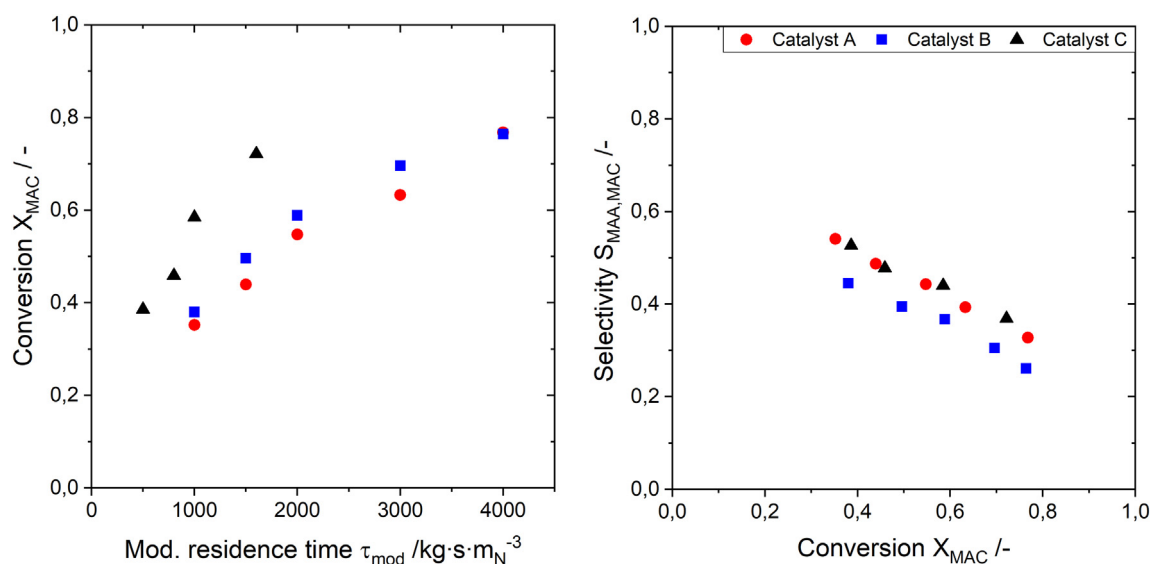
Fig. 4. Catalytic performances of the three catalysts. MAC conversion over the modified residence time (left), MAA selectivity over MAC conversion (right).

Table 2
Mass specific, surface specific and crystallinity corrected mass specific catalyst activity coefficients for catalysts A, B and C.

Catalyst	k $(m^3/kg/s)$	$k_F(m/s)$	$k_C(m^3/kg/s)$
A	$5.17 \cdot 10^{-4}$	$3.71 \cdot 10^{-8}$	$6.55 \cdot 10^{-4}$
B	$5.55 \cdot 10^{-4}$	$2.69 \cdot 10^{-8}$	$8.16 \cdot 10^{-4}$
C	$1.17 \cdot 10^{-3}$	$4.52 \cdot 10^{-8}$	$2.01 \cdot 10^{-3}$

phase was only known for its catalytic activity in the partial oxidation of acrolein to acrylic acid. Interestingly, all the tested catalyst exceed the typical performance of Mo/V/W mixed oxides in the partial oxidation of methacrolein as reported by literature [2]. The hexagonal $(Mo,V,W)O_3$-phase is stable under typical reaction conditions and shows a similar selectivity towards methacrylic acid compared to the M1 phase. These findings are in contradiction to the current literature knowledge, which considers nanocrystalline/amorphous M1- and Mo_5O_{14}-phases as the selective species in the partial oxidation of unsaturated aldehydes such as acrolein and methacrolein [2,9,19]. Further research will be required to identify relationships between structure and catalytic performance.

Declaration of Competing Interest

The authors declare that they have no known competing financial interests or personal relationships that could have appeared to influence the work reported in this paper.

Appendix A. Supplementary data

Supplementary data to this article can be found online at https://

doi.org/10.1016/j.catcom.2020.106016.

References

[1] Ullmann's Encyclopedia of Industrial Chemistry, Wiley-VCH Verlag GmbH & Co. KGaA, Weinheim, Germany, (2012).

[2] A. Drochner, D. Ohlig, S. Knoche, N. Gora, M. Heid, N. Menning, T. Petzold, H. Vogel, Mechanistic studies on the transition metal oxide catalysed partial oxidation of (meth)Acrolein to the corresponding carboxylic acids, Top. Catal. 59 (2016) 1518–1532, https://doi.org/10.1007/s11244-016-0670-3.

[3] H. Böhnke, J. Gaube, J. Petzoldt, Selective Oxidation of Methacrolein towards Methacrylic Acid on Mixed Oxide (Mo, V, W) Catalysts. Part 1, Studies on Kinetics, Industrial and Engineering Chemistry Research 45 (2006) 8794–8800, https://doi.org/10.1021/ie060499r.

[4] H. Böhnke, J. Gaube, J. Petzoldt, Selective Oxidation of Methacrolein towards Methacrylic Acid on Mixed Oxide (Mo, V, W) Catalysts. Part 2. Variation of Catalyst Composition and Comparison with Acrolein Oxidation, Ind. Eng. Chem. Res. 45 (2006) 8801–8806, https://doi.org/10.1021/ie060500m.

[5] C. Chen, N. Kosuke, T. Murayama, W. Ueda, Single-crystalline-phase Mo_3VO_x an efficient catalyst for the partial oxidation of Acrolein to acrylic acid, ChemCatChem 5 (2013) 2869–2873, https://doi.org/10.1002/cctc.201300268.

[6] M. Dieterle, G. Mestl, J. Jäger, Y. Uchida, H. Hibst, R. Schlögl, Mixed molybdenum oxide based partial oxidation catalyst, J. Mol. Catal. A Chem. 174 (2001) 169–185, https://doi.org/10.1016/S1381-1169(01)00074-7.

[7] H. Hibst, F. Rosowski, G. Cox, New Cs-containing Mo–V4+ based oxides with the structure of the M1 phase—base for new catalysts for the direct alkane activation, Catal. Today 117 (2006) 234–241, https://doi.org/10.1016/j.cattod.2006.05.045.

[8] P. DeSanto, D.J. Buttrey, R.K. Grasselli, C.G. Lugmair, A.F. Volpe, B.H. Toby, T. Vogt, Structural aspects of the M1 and M2 phases in MoVNbTeO propane ammoxidation catalysts, Zeitschrift für Kristallographie - Crystalline Materials 219 (2004) 40, https://doi.org/10.1524/zkri.219.3.152.29091.

[9] C. Qiu, C. Chen, S. Ishikawa, Z. Zhang, T. Murayama, W. Ueda, Synthesis of crystalline Mo–V–W–O complex oxides with orthorhombic and trigonal structures and their application as catalysts, Catalysis, Structure & Reactivity 1 (2015) 71–77, https://doi.org/10.1179/2055075814Y.0000000009.

[10] C. Qiu, C. Chen, S. Ishikawa, T. Murayama, W. Ueda, Crystalline Mo-V-W-mixed oxide with orthorhombic and Trigonal structures as highly efficient oxidation catalysts of Acrolein to acrylic acid, Top. Catal. 57 (2014) 1163–1170, https://doi.org/10.1007/s11244-014-0283-7.

[11] J. Kunert, Untersuchungen zur Acroleinoxidation am Mo/V/W-Mischoxidsystem - Über die Präparationsstrategie zum katalytischen Verständnis, Technische Universität Darmstadt, 2003.

[12] J. Kunert, A. Drochner, J. Ott, H. Vogel, H. Fueß, Synthesis of Mo/V mixed oxide catalysts via crystallisation and spray drying - a novel approach for controlled preparation of acrolein to acrylic acid catalysts, Appl. Catal. A Gen. 269 (2004) 53–61, https://doi.org/10.1016/j.apcata.2004.03.050.

[13] H. Hibst, A. Tenten, L. Marosi, (BASF SE) DE19542755A1, (1997).

[14] F. Rosowski, K.J. Müller-Engel, J. Klaus, N. Blickhan, N. Dürr, T. Jekewitz, N. Menning, T. Petzold, S. Schmidt, (BASF SE;) DE102012207811A1, (2012).

[15] S. Endres, P. Kampe, J. Kunert, A. Drochner, H. Vogel, The influence of tungsten on structure and activity of Mo–V–W-mixed oxide catalysts for acrolein oxidation, Appl. Catal. A Gen. 325 (2007) 237–243, https://doi.org/10.1016/j.apcata.2007.02.040.

[16] Y. Hu, P.K. Davies, Synthesis, Thermal Stability, and Structure of $(V_{.13}Mo_{.87})O_{2.935}$: A New Oxide with the Open Hexagonal MoO3 Structure, J. Solid State Chem. 105 (1993) 489–503, https://doi.org/10.1006/jssc.1993.1241.

[17] F.I.Z. Karlsruhe, ICSD, https://icsd.fiz-karlsruhe.de.

[18] W. Ueda, Establishment of crystalline complex Mo–V–oxides as selective oxidation catalysts, J. Jpn. Petrol. Inst. 56 (2013) 122–132, https://doi.org/10.1627/jpi.56.122.

[19] O. Ovsitser, Y. Uchida, G. Mestl, G. Weinberg, A. Blume, J. Jäger, M. Dieterle, H. Hibst, R. Schlögl, Molybdenum oxide based partial oxidation catalyst, J. Mol. Catal. A Chem. 185 (2002) 291–303, https://doi.org/10.1016/S1381-1169(02)00128-0.